Journal of Inorganic and General Chemistry
ZAAC
Zeitschrift für anorganische und allgemeine Chemie

DOI: 10.1002/zaac.201800097

ARTICLE

Solid-state and Computational Study of “Venus fly-trap” Geometric Parameters for 1,5-Cyclooctadiene in Pd^{II} and Pt^{II} β-Enaminonato Complexes

Tania N. Hill[a] and Andreas Roodt*[a]

Dedicated to Prof Peter Comba on the Occasion of his 65th Birthday

Abstract. The cod ligand (*cis*,*cis*-1,5-cyclooctadiene) can be superficially considered to mimic similarities in spatial behavior of a leaf of the Venus fly-trap (*Dionaea muscipula*). Thus, the synthesis of an unsymmetrical bidentate *trans* ligand (*N*,*O*-donor atoms) based on the β-enaminonate backbone is introduced to evaluate the electronic and steric influence on the structural behavior of the *cod* ligand when coordinated to a square planar transition metal. A range of platinum(II) / palladium(II) complexes of the type [*M*(cod)(*N*,*O*-Bid)]*A* (M = Pt^{II}, Pd^{II}; β-enaminonato ligand (*N*,*O*-Bid) = NH-acac, NMe-acac, NPh-acac; A = BF_4^-, PF_6^-) is reported. The complexes were fully characterized, including by detailed X-ray structural investigations. Theoretical calculations on the [*M*(cod)(*N*,*O*-Bid)]$^+$ complexes for the complete nickel triad are also described and the structural behavior of the cod ligand critically evaluated. The influence of the variation of the β-enaminonato ligands on the coordination arrangement of the cod was investigated and found that no significant changes to the *M*–C and C=C bond lengths were observed. The Venus fly-trap jaw angle (ψ), however, varies by ca. 8° and the twist angle (τ) by ca. 10°, whereas the cod bite angle (χ), as well as the β-enaminonato ligand bite angle (N–M–O; θ) both remain virtually constant. Calculated spectroscopic tendencies within the Ni-triad are also included.

Introduction

The compound, *cis*,*cis*-1,5-cyclooctadiene (cod) is a cyclic diolefin, which is often utilized as a precursor ligand in organic type reactions, serving as a weak coordinating entity in organometallic chemistry.[1] It is also an important substrate in industrial reactions[2] and is utilized in a variety of chemical processes from catalysis[3] to pharmaceuticals and model diolefin complexes.[4] In some petrochemical processes diolefins can also act as catalyst trapping agents/ inhibitors and thus quantification of aspects which defines its coordination to transition metals are critically important.

The two most common conformers of cod are the boat and chair configurations, and their well-known ability of coordinating with middle to late transition metals is broadly documented,[5] generally accompanied by the formation of halido complexes. Cod also forms complexes with central metal atoms bearing *O,O′*- and *N*,*O*-bidentate ligands, although only a few of the latter have been synthesized and characterized.

It however further exhibits an additional interesting aspect, i.e., to broadly structurally “mimic” the Venus fly-trap behavior (*Dionaea muscipula*);[6] at least the jaw movement (not the actual eating of insect subjects!) To clarify this statement: when one observes a 3D diagram of cyclooctadiene coordinated to a transition metal it is clearly possible to visualize the structure of the leaf of the Venus fly-trap plant, mimicking the configuration of the cod.

Three parameters to describe the behavior of the cod ligand as a “leaf” of the Venus fly-trap can thus be loosely defined, namely the ψ or cod *jaw* angle, the χ or cod *bite* angle and the *twist* angle or τ, as illustrated in Figure 1.[7] A fourth parameter utilized but not illustrated since it is not formally part of the “leaf” is the N–M–O bite angle of the β-enaminonato ligand (θ), *trans* to the cyclooctadiene.

In this paper we present low-temperature crystal structures of several platinum(II) / palladium(II) cod β-enaminonato complexes of the type [*M*(cod)(*N*,*O*-Bid)]*A* (M = Pt^{II}, Pd^{II}; *N*,*O*-Bid = NH-acac, NMe-acac, NPh-acac; A = BF_4^-, PF_6^-), wherein we carefully examine the influence of the bidentate ligand donor atoms on the pre-defined “Venus fly-trap” parameters. Furthermore, we present DFT calculations on the [*M*(cod)(*N*,*O*-Bid)]$^+$ complexes for the nickel triad, to further the understanding of the coordination model of cod down the series, and the electronic influence that the β-enaminonato ligand systems have on the distortion within the cod ligand. In this regard we additionally opted to vary the counterion of two complexes to evaluate the possible effect thereof. We thus critically correlate the solid-state structural behavior of the cod as defined by the Venus fly-trap parameters as a function of the *trans* β-enaminonato ligand and expand it across the complete Ni-triad using computational chemistry to observe and attempt to account for the geometric changes observed.

---

* PhD. A. Roodt
[a] Department of Chemistry
University of the Free State
Bloemfontein 9300, South Africa

Supporting information for this article is available on the WWW under **http://dx.doi.org/10.1002/zaac.201800097** or from the author.

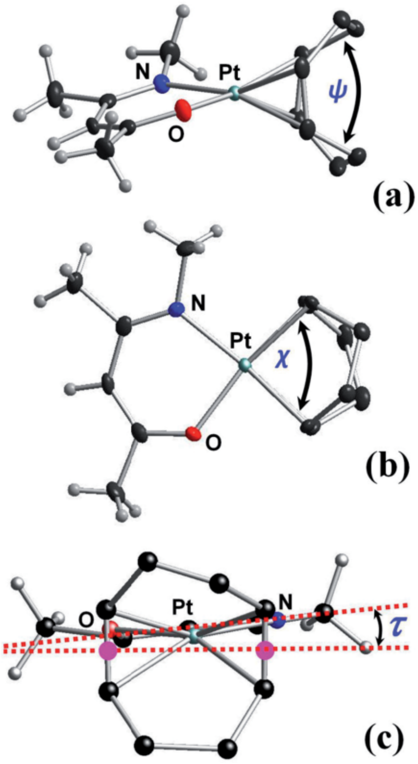

Figure 1. Definition of the three angles describing the arrangement of the cod ligand: (a) ψ, opening of the Venus fly-trap "**jaw**": dihedral angle between the two planes through the alkane carbon fragments of the cyclooctadiene moiety; (b) χ, the "**bite**" of the Venus fly-trap: dihedral angle between the two olefinic moiety-metal atom planes; (c) τ, the **twist** angle: dihedral angle between the plane through the *trans* bidentate ligand and the plane through the mid-points of the alkene carbons of cod (illustrated by pink dummy atoms).

Results and Discussion

Synthesis

The starting compounds were synthesized by previously reported procedures. For dichlorido(1,5-cyclooctadiene)platinum(II),[8] a solution containing potassium tetrachloridoplatinate in a mixture of water and propanol with an addition of an excess of *cis*,*cis*-1,5-cyclooctadiene (cod) followed by a catalytic amount of tin chloride was stirred for several days and allowed to evaporate to dryness. The [Pt(cod)Cl_2] was subsequently extracted with dichloromethane. For [Pd(cod)Cl_2],[9] palladium dichloride was dissolved in concentrated hydrochloric acid and diluted with ethanol; after the addition of an equivalent of cod, the mixture was filtered and dichlorido(1,5-cyclooctadiene)palladium(II) was obtained. The most general method for synthesizing β-enaminonato ligands involves the condensation between either ammonia or a secondary amine and a 1,3-diketone (Scheme 1). The β-enaminoketones **1**–**3** were prepared in high yields (ca. 70–90 %) by the condensation of acetylacetone (pentane-2,4-dione, Hacac) with the respective amine.

By using a modified synthetic procedure described by *White*,[33] the palladium(II) and platinum(II) complexes **4**–**11** were synthesized utilizing either dichloro(1,5-cyclooctadiene)palladium(II) or dichloro(1,5-cyclooctadiene)platinum(II) dissolved in dichloromethane, adding a silver salt to remove the chloride ions via filtration, then followed by an equivalent of a β-enaminonato ligand (**1**–**3**). The mixture was filtered, and the product was precipitated by the addition of diethyl ether (Scheme 1). The yield deviation of the β-enaminonato complexes was found to be similar to the β-diketonato complexes,[10] in that the tetrafluoroborate (BF_4^-) complexes have a marginally lower yield than their hexafluorophosphate (PF_6^-) counterparts. The variation is attributed to the increase in stability and hydrogen bonding interactions of the coordinating anion (Figure S1, Supporting Information). Additionally, the donor atom of the coordinating ligand plays a role, as mentioned in the hard and soft acid and base (HSAB) theory oxygen is a *hard base* whilst palladium(II) / platinum(II) fall into the *soft acid* category. With the introduction of a nitrogen donor atom replacing one of the oxygen donors, the ligand takes on *soft base* characteristics. All the compounds were obtained in reasonable yields, and characterized by IR, ^1H and ^{13}C NMR spectroscopy and crystals suitable for X-ray crystallographic analysis were obtained by dichloromethane / diethyl ether vapor diffusion.

X-ray Structural Investigations

The central palladium and platinum metal atoms of complexes **4**, **6**–**11** are bonded by the nitrogen and oxygen atoms of the β-enaminonato ligand and π-bonded by the two alkene fragments of the cod ligand, resulting in a distorted square-planar coordination arrangement around the transition metal atom. The cationic nature of the synthesized complexes and the resulting charge was balanced by the use of either tetrafluoroborate (BF_4^-) or hexafluorophosphate (PF_6^-) ions. The ions display classic tetrahedral and octahedral arrangements with a positional disorder only found for **4** and **9**, whereas the remaining counterions were well behaved. The molecular structures of four complexes are illustrated in Figure 2, with selected bond lengths and angles reported in Table 1.

A search of the Cambridge structural database (CSD, ver 5.36) [11] with a six-membered metal chelate ring using plati-

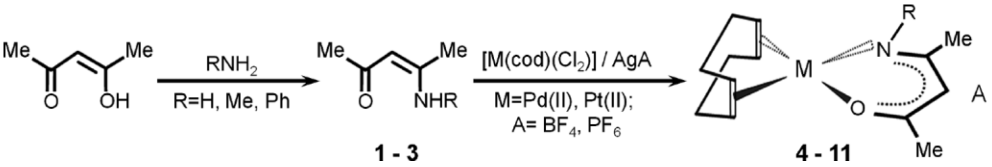

Scheme 1. Simplified reaction sequence for the synthesis of compounds **1**–**11**.

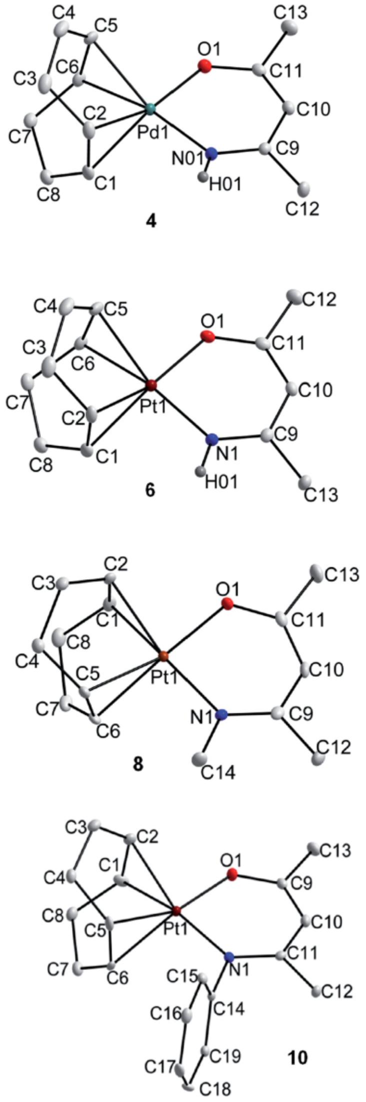

Figure 2. Anisotropic displacement parameter plots (30 % probability) of **4**, **6**, **8**, and **10** depicting the atomic numbering scheme; only selected hydrogen atoms are shown.

num and palladium as the central metal yielded 679 hits; of these 174 were for platinum and the remaining 505 hits for palladium. The majority of the structures were based on variations of Schiff base ligands. The average distances and angles obtained for platinum(II) were Pt–N 1.997(30) Å, Pt–O 2.006(22) Å, and N–Pt–O angles of 92.931(1.787)° whilst, for palladium(II) Pd–N 2.006(34) Å, Pd–O 2.012(38) Å, and N–Pd–O of 92.039(1.758)° were found. In refining the search, incorporating cod as an additional ligand to the six membered chelate *N*,*O*-bidentate ligand previously searched, only two structures were found and are reported by *Boyer* et al.;[12] both structures comprise of a functionalized aminophenol ligand.

The β-enaminone ligands have as yet not been structurally characterized with neither platinum nor palladium cod complexes. However, a number of *O*,*O*-Bid (including β-diketonato) complexes of platinum and palladium have been reported.[11] Relevant selected solid-state data for the β-enaminonato complexes of Pd^{II} and Pt^{II} described in this study, are summarized in Table 1. Before discussing this in detail however, the packing modes within these compounds are briefly considered.

Hydrogen bond interactions for **4** and **6–11** are listed in Tables S1 and S2 (Supporting Information), whereas representative illustrations of the hydrogen bonding for **4**, **7**, and **8** are given in Figure S1 (Supporting Information). Hydrogen interactions are mostly observed between the fluorido moieties of the counterions and the complexes themselves (Figure S1a shows a classic example of a bifurcated hydrogen, H_5). Metal chelate ring···metal chelate ring interactions were observed for **4** and **6** with distances of 3.5513(1) Å and 3.5561(1) Å, with symmetry operators of [2–*x*, 1 –*y*, 1 –*z*] and [1–*x*, –*y*, 1 –*z*] respectively, illustrated in Figure 3a. Similarly, for **8**, a metal chelate ring hydrogen interaction was found with the methyl hydrogen (H_{12C} and H_{12A}) of the β-enaminonato ligand with distances of 2.9147(1) Å and 3.2013(1) Å and symmetry operators of [1–*x*, –1/2 + *y*, 3/2 –*z*] and [1/2 –*x*, –*y*, 1/2 + *z*], respectively (Figure 3b).

Table 1. Selected crystallographic bond lengths /Å and angles /° for complexes **4**, **6–11**.

	4	**6**	**7**	**8**	**9**	**10**	**11**
$M–O_1$	1.998(1)	2.009(2)	1.995(7)	1.984(2)	1.972(3)	1.989(3)	1.99(1)
$M–N_1$	1.972(2)	1.978(3)	1.996(6)	2.035(2)	2.047(3)	2.033(4)	2.07(1)
$M–C_1$	2.184(2)	2.152(3)	2.188(5)	2.187(3)	2.166(3)	2.186(5)	2.17(2)
$M–C_2$	2.210(2)	2.168(3)	2.188(5)	2.180(3)	2.166(3)	2.196(5)	2.19(2)
$M–C_5$	2.219(2)	2.183(3)	2.143(5)	2.178(3)	2.192(3)	2.184(4)	2.09(3)
$M–C_6$	2.226(2)	2.187(3)	2.143(5)	2.161(3)	2.192(3)	2.171(4)	2.17(2)
$C_1–C_2$	1.382(3)	1.395(5)	1.385(15)	1.388(4)	1.385(8)	1.417(6)	1.45(3)
$C_5–C_6$	1.374(3)	1.396(5)	1.385(15)	1.396(4)	1.396(7)	1.403(6)	1.42(3)
$C_1–M–C_2$	36.66(8)	37.7(1)	36.9(4)	37.06(10)	37.1(2)	37.7(2)	38.7(9)
$C_5–M–C_6$	36.00(8)	37.2(1)	36.9(4)	37.52(11)	37.0(2)	37.6(1)	38.9(8)
$C_1–M–C_6$	82.14(7)	82.7(1)	82.3(2)	81.56(11)	$^{\mathrm{i)}}$	80.8(2)	80.9(9)
$C_2–M–C_5$	81.79(8)	82.1(1)	82.3(2)	81.67(10)	$^{\mathrm{i)}}$ 80.97(13)	80.7(1)	79.6(11)
θ ($O_1–M–N_1$)	91.84(6)	91.5(1)	91.8(3)	92.12(8)	92.28(14)	91.7(1)	92.6(5)
χ (cod bite)	86.4(1)	87.2(2)	87.8(2)	86.35(8)	86.3(1)	85.3(2)	86.1(9)
ψ (cod jaw)	83.8(1)	78.6(2)	80.7(4)	78.5(1)	81.4(2)	78.4(2)	75.8(13)
τ (twist)	3.3(1)	3.8(2)	0	10.9(2)	0	3.6(2)	5.3(6)

Symmetry operator: i) [*x*, –*y*, *z*].

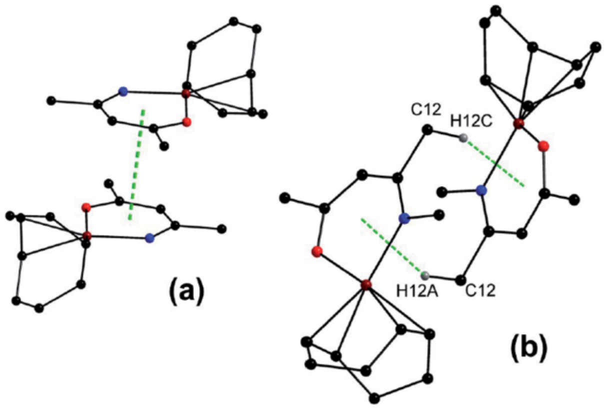

Figure 3. Molecular diagram of (a) compound **6**, illustrating metal chelate ring interactions by dashed bonds. Symmetry operator [1–*x*, –*y*, 1 –*z*]; (b) compound **8**, illustrating H···metal chelate ring interactions by dashed bonds. Symmetry operators [1–*x*, –1/2 + *y*, 3/2 –*z*], [1/2 –*x*, 1 –*y*, 1/2 + *z*]. Counter ions and hydrogen atoms are omitted for clarity.

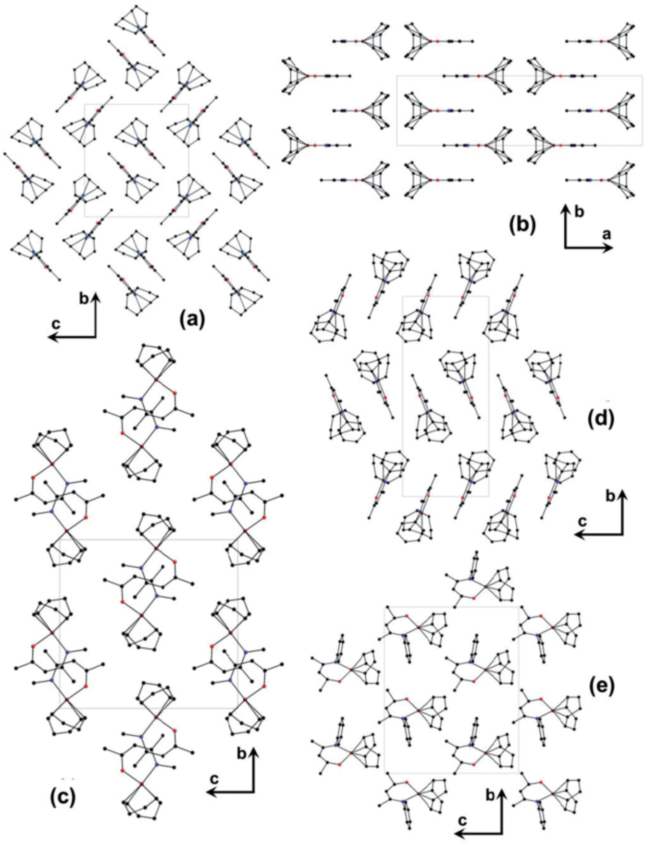

Figure 4. Packing mode illustrations of (a) clustered head-to-tail for **4** and **6**, (b) head-to-head for **7** and **9**, (c) clustered tail-to-tail for **8**, (d) head-to-tail for **10**, and (e) head-to-tail for **11**. Counter-ions and hydrogen atoms are omitted for clarity.

A clustered head-to-tail packing was observed for the isomorphous complexes of **4** and **6**, whereas the isostructural complexes of **7** and **9** were seen to have a classic head-to-tail packing with a clear linear delineation (see Figure 4a and b, respectively). The H···metal chelate ring interaction is also a primary consequence for the clustered tail-to-tail packing found in **8** (Figure 4c).

The remaining complexes showed head-to-tail packings: for **10** a zigzag in the overlying structure is observed, whereas **11** showed a more random arrangement viewed along the *b* axis (Figure 4d and e). Naturally, the significant steric contribution from the phenyl ring on the NPh-acac ligand is presumably responsible for this latter packing mode (Figure 4e).

The solid-state data for the β-enaminonato complexes of Pd^{II} and Pt^{II} agree well with each other, as manifested in the general bonds and angles within the *N*,*O*-Bid ligand yielding very similar bond lengths therein, as well as similar bonding modes as defined by the O–*M*–N bite angles (θ) of around 91.5–92.6° (see Table 1). The influence of both the metal chelate ring and the H···metal chelate ring interactions along with the hydrogen bonding interactions of the counterions do not significantly affect the Venus fly-trap angles. A minor increase in the *M*–N bond lengths was observed as the electron donating ability of the ligands was increased. As for *M*–O, C=C and *M*–C bond lengths these did not show any appreciable changes (Table 1).

It was envisaged that with the incorporation of the nitrogen donor atom in the *N*,*O*-Bid ligand, the asymmetry of the coordinating bidentate ligand will influence the Venus fly-trap angles of the complexes. Thus, these parameters as defined in Figure 1, using the solid-state data obtained from the crystallographic studies, and as illustrated in Figure 5 (data from Table 1), shows emerging geometric tendencies within the cyclooctadiene ligand. Although the O–*M*–N bite angle (θ) stays virtually constant, there is a systematic increase in the ψ (jaw) from the N–Ph substituents (around 76–78°) to the mixed N–Me and N–H complexes of 79–84°. A total increase of ca. 8° was thus observed with the more bulky N–Ph substituents showing the smallest ψ (jaw) angle variation on the cod. The cod bite angle χ, on the other hand also stays fairly constant at around 86–87°. This is to be expected due to the lanthanide contraction from the 4th to the 5th row transition series, yielding very similar ion radii for the Pd^{II} and Pt^{II}. Thus, only the

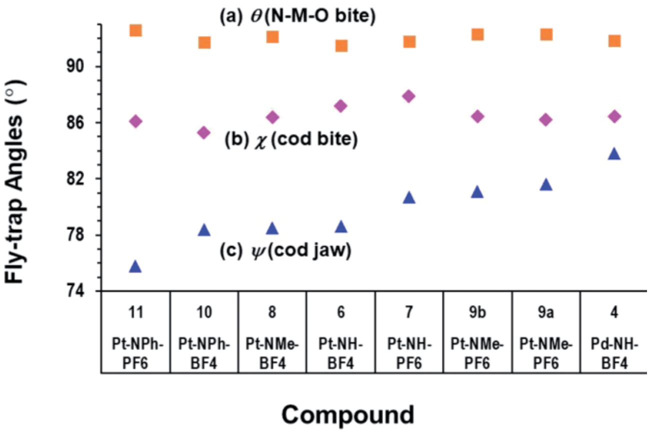

Figure 5. Graph of the Venus fly-trap angles observed from single crystal data for $[M(cod)(N,O\text{-Bid})]^+$ (*M* = Pd, Pt; *N*,*O*-Bid = NH-acac, NMe-acac, NPh-acac). (a) θ (N–*M*–O enaminonato bite) (b) χ (cod bite), and (c) ψ (cod jaw) (°) (see Table S3, Supporting Information).

jaw angle, i.e., the opening/ closing of the "mouth" of the Venus fly-trap varies significantly, assumed indicative of the *electronic* changes of the N-substituents H, Me, and Ph.

The fly-trap angles are predominantly defined on the core coordination arrangement with a presumably small contribution from the counterion. The latter was observed for the ψ (jaw) angle in the complexes containing the BF_4^- ion to have a slightly smaller value than those with the PF_6^- ions (Table 1) as in **6** and **7** (NMe-acac) and **8** and **9** (NMe-acac), respectively. However, the opposite holds true in **10** and **11**, where the PF_6^- salt exhibits the smallest ψ (jaw) angle.

These parameters within the complexes, including the twist angle (τ), are further discussed under the computational study following the incorporation of the DFT optimized data of the complete Ni-triad.

Spectroscopy

The IR spectra of the compounds showed characteristic bands at 635–664 cm^{-1} and 416–474 cm^{-1} assigned to ν(Pt–O) + Δ(ring) (in-plane ring distortion) and ν(Pt–O), while ν(Pt–[C=C]) were found at 521–557 cm^{-1}. For the ν(Pt–O) the effect of the counter ligand is inconsequential, however, the change in the *R* group on the N atom leads to a downfield shift of ca. 29 cm^{-1} as the electron donating ability of the *R* group is increased.

The resonances of the methine hydrogen atoms of the cyclooctadiene demonstrated the classic triplet of ^{195}Pt complexes, and multiplets were observed for the ^{105}Pd complexes. For the β-enaminonato hydrogen (H_{10}) an increase in the proton shift from 5.33 ppm to 5.62 ppm was found consistent with the increase electron with-drawing properties of the ligand. Along with the vicinal coupling seen for both **4** and **5**, resulting in the splitting of the multiplets into a doublet of multiplets for the olefinic hydrogens, the influence of the scalar hydrogen bond coupling ($^{H1}J_{HF}$) on **4** can be clearly seen by the increased splitting (Figure S2, Supporting Information, whereas Figure S1a illustrates the hydrogen bonding of **4**). The $^{13}C\{^1H\}$ NMR resonances (Experimental Section) are in accordance with the proposed structures.

Computational Results

Geometry Optimization

Accurate relevant solid-state data for the isostructural complexes of all the members is not available for comparison as difficulties in isolating and crystallizing the complexes proved quite a challenge; for the Pd^{II} but in particular with the Ni^{II}. Therefore, DFT calculations were performed to compare the arrangement with the obtained complexes **4**, **6–11**. The DFT optimized structures are indicated by a "C" following the complexes' structure abbreviation. In addition, the complete nickel triad was used for DFT studies to gain further insight into the bonding nature of these complexes. An excellent correlation between the computed structures and that of the experimental structures was obtained as can be seen in Figure 6, which presents selected HyperChem™ superimposed images of **4**, **8**, and **10** with the calculated $[Pd(cod)(NH\text{-}acac)]^+$, $[Pt(cod)(NMe\text{-}acac)]^+$, and $[Pt(cod)(NPh\text{-}acac)]^+$ moieties, yielding *r.m.s.* values of only 0.07 Å, 0.13 Å and 0.02 Å.

The *r.m.s.* values for the remaining complexes **6**, **7**, and **11** with their respective calculated complexes were calculated as 0.13 Å, 0.16 Å, and 0.16 Å, respectively. Due to the disorder for **9** (Figure S3, Supporting Information), two *r.m.s.* values were calculated for the respective parts of the disorder namely 0.22 Å and 0.18 Å, the major difference in the overlay being in the disordered carbon (C_3) of the cod.

In general, the optimized geometric parameters are in very good agreement with the values based upon the X-ray crystal structure data (see Figure 7 and Table 2), and the common trends observed in the experimental data are reproduced in the calculations. It should however be noted that the theoretical calculations do not consider the effects of the chemical environment for example intermolecular packing interactions. As a result, the distances for the theoretical calculations are fractionally longer (1–3 %) than those observed for the X-ray crystal structures.

The Venus fly-trap parameters were also obtained from the DFT calculations, and these together with those obtained from the solid-state crystallographic work are summarized in Table 3.

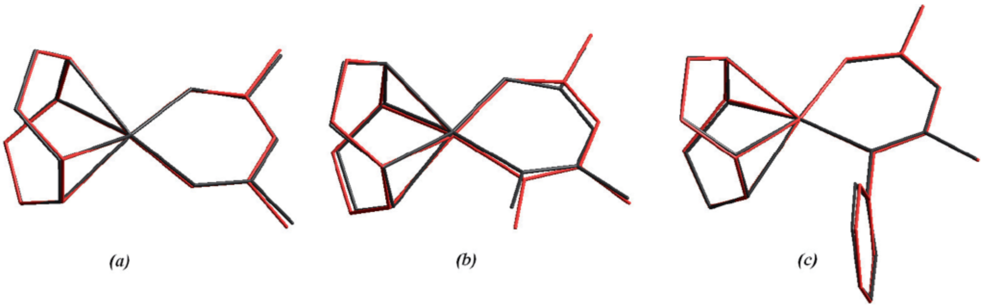

Figure 6. HyperChem™ superimosed image of (a) **4** (black) vs. $[Pd(cod)(NH\text{-}acac)]^+$ (calculated) (red) with an *r.m.s.* error of 0.07 Å, (b) **8** (black) vs. $[Pt(cod)(NMe\text{-}acac)]^+$ (calculated) (red) with an *r.m.s.* error of 0.13 Å, and (c) **10** (black) vs. $[Pt(cod)(NPh\text{-}acac)]^+$ (calculated) (red) with an *r.m.s.* error of 0.02 Å. The counterions and hydrogen atoms of the X-ray crystal structures are omitted for clarity.

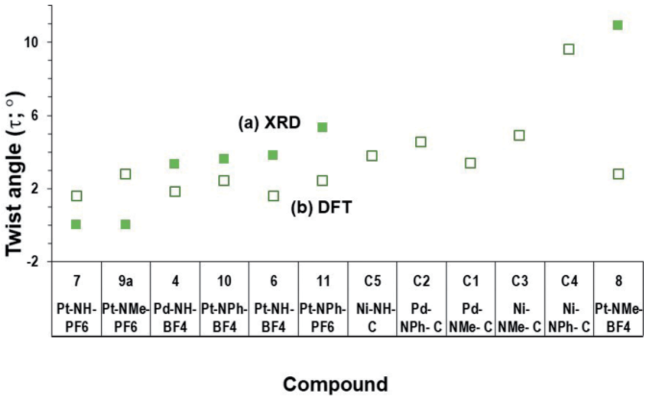

Figure 7. Graph of the twist angle τ (°): (a) computed values (open symbols); compared to (b) crystallographically observed (filled symbols); for $[M(\text{cod})(N,O\text{-Bid})]^+$ (M = Ni, Pd, Pt; N,O-Bid = NH-acac, NMe-acac, NPh-acac) (see Table S4, Supporting Information).

Next, the distortion from the square-planar arrangement was probed by the twist angle τ (Figure 1c), i.e. the dihedral angle between the planes defined by the metal atom and the midpoints of the alkene carbons of the cod ring on the one hand, and the metal atom and the O and N atoms of either the 4-amino, 4-methylamino, and 4-anilinopent-3-en-onato ligand, on the other. A general increasing trend is observed with **8** showing the largest distortion of 10.9(5)° (see Table 2). The trend in the twist angle is illustrated in Figure 7, relating it to the DFT results. Although a significant trend, it is unclear exactly what the reason is, although it is known that nickel(II) sometimes favors a tetrahedral arrangement and indications are that the twist is more prominent therein. Changing the counterion influences the distortion, but no discernible trend was observed as alluded to above.

Encouraged by the trends observed from Figure 5, the individual computational fly-trap parameters were next correlated with that observed from the solid-state data (see Figure 8).

The increasing trend of the ψ (jaw) angle in Figure 8a is somewhat maintained by the DFT results, albeit less pronounced, for reasons not perfectly clear. Nevertheless, all being equal, it underlines the fact that the ψ angle of the cod as defined, opens/ closes when electronic changes at the central metal atom occurs.

The best agreement between the XRD and the computed results is within the N–*M*–O bite angles, which are clearly very good (Figure 8c). An interesting observation is the fact that the cod bite angle (χ) seems to constantly follow a ca. 2° smaller value for the DFT data compared to the crystallographic data (see Figure 8b). A reason for this is potentially observable in the four *M*–C bonds for the cod ligand. These are all ca. 0.02 to 0.06 Å longer than the corresponding crystallographic data (Table 2), which might suggest that the DFT is not able in this case to accurately model the distorted olefin interactions with the central metal atoms; at least in these examples presented.

Table 2. Selected average crystallographic and DFT optimized bond lengths /Å and angles /° for complexes **4** and **6–11**.

Bond/angle	Pd(cod)-(NH-acac)		Pt(cod)-(NH-acac)		Pt(cod)-(NMe-acac)		Pt(cod)-(NPh-acac)	
	XRD, **4**	Calcd.	XRD$_{avg}$, **6** and **7**	Calcd.	XRD, **8** and **9**	Calcd.	XRD$_{avg}$, **10** and **11**	Calcd.
M–O_1	1.998(1)	2.024	2.002(4)	2.033	1.978(3)	2.024	1.990(2)	2.030
M–N_1	1.972(2)	2.012	1.987(4)	2.013	2.041(3)	2.069	2.052(3)	2.070
M–C_1	2.184(2)	2.266	2.180(4)	2.215	2.177(3)	2.233	2.178(3)	2.234
M–C_2	2.210(2)	2.242	2.178(4)	2.201	2.173(3)	2.211	2.193(3)	2.218
M–C_5	2.219(2)	2.309	2.163(4)	2.261	2.185(3)	2.260	2.137(4)	2.263
M–C_6	2.226(2)	2.279	2.165(4)	2.241	2.176(3)	2.244	2.171(3)	2.243
C_1–C_2	1.382(3)	1.385	1.390(10)	1.402	1.387(6)	1.400	1.434(5)	1.399
C_5–C_6	1.374(3)	1.377	1.391(10)	1.391	1.396(6)	1.393	1.412(5)	1.393
O_1–M–N_1	91.84(6)	90.85	91.6(2)	90.41	92.21(5)	92.08	92.2(3)	91.78
C_1–M–C_2	36.66(8)	35.78	37.3(3)	37.01	37.1(1)	36.72	38.2(6)	36.64
C_5–M–C_6	36.00(8)	34.93	37.1(3)	36.00	37.3(2)	36.02	38.3(5)	36.01
C_1–M–C_6	82.14(7)	80.50	82.5(2)	81.00	81.56(11)	79.95	80.9(5)	80.15
C_2–M–C_5	81.79(8)	80.24	82.2(2)	80.80	81.37(10)	80.14	80.2(6)	79.94

Table 3. Venus Fly-trap parameters from crystallographic and DFT study.

Parameter	Pt-NPh-$PF_6$$^{b)}$ **11**	Pt-NPh-BF_4 **10**	Pt-NMe-BF_4 **8**	Pt-NH-BF_4 **6**	Pt-NH-PF_6 **7**	Pt-NMe-PF_6 **9b**	Pt-NMe-PF_6 **9a**	Pd-NH-BF_4 **4**	Pd-NMe-C **C1**	Pd-NPh-C **C2**	Ni-NMe-C **C3**	Ni-NPh-C **C4**	Ni-NH-C **C5**
χ, cod bite$^{a)}$	86.1	85.3	86.4	87.2	87.9	86.4	86.2	86.4	–	–	–	–	–
$\chi_c$$^{c)}$	84.3	84.3	84.3	85.3	85.3	84.3	84.3	84.3	82.9	82.9	83.0	83.4	85.9
ψ, cod jaw$^{a)}$	75.8	78.4	78.5	78.6	80.7	81.1	81.6	83.8	–	–	–	–	–
ψ_c^{c}	82.6	82.6	82.1	82.4	82.4	82.1	85.5	82.1	85.2	85.7	86.2	86.6	86.1
θ, N–M–O bite$^{a)}$	92.6	91.7	92.1	91.5	91.8	92.3	92.3	91.8	–	–	–	–	–
$\theta_c$$^{c)}$	91.9	91.9	92.1	90.4	90.4	92.1	92.1	90.9	92.5	92.2	94.3	93.9	93.1
τ, twist angle$^{a)}$	5.3	3.6	10.9	3.8	0	0	0	3.3	–	–	–	–	–
$\tau_c$$^{c)}$	2.4	2.4	2.8	1.5	1.5	2.8	2.8	1.8	3.4	4.5	4.9	9.6	3.8

a) e.s.d.'s for all XRD values ca 0.1–0.2 degrees. b) e.s.d.'s for **11** ca. 1 degree. c) Calculated values using cation only.

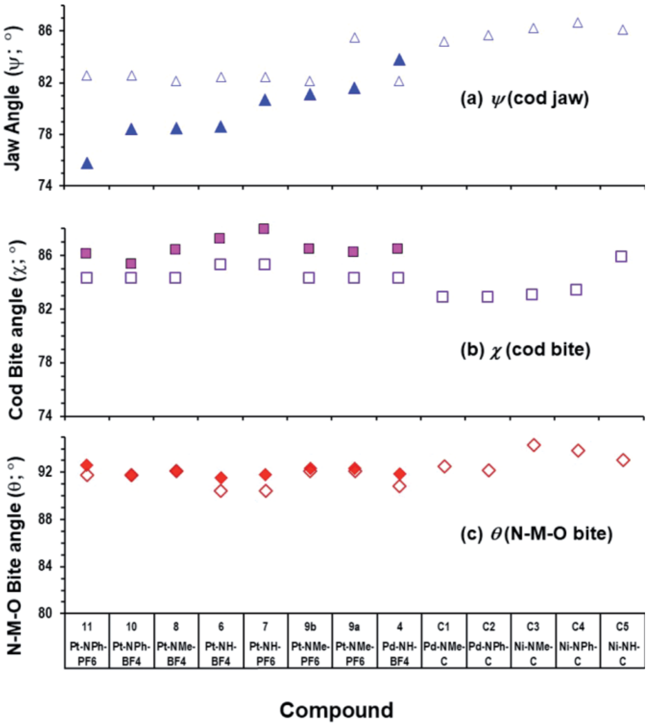

Figure 8. Graph of the Venus fly-trap angles (°) (a) ψ (cod jaw), (b) χ (cod bite), (c) the θ (N–*M*–O enaminonato bite): computed values (open symbols) vs. crystallographically observed (filled symbols) for [*M*(cod)(*N*,*O*-Bid)]$^+$ (*M* = Ni, Pd, Pt; *N*,*O*-Bid = NH-acac, NMe-acac, NPh-acac) (see Table S4, Supporting Information).

Orbitals

A visual representation of the nature of the bonding mode is given through the use of the molecular orbitals (MOs). The second-highest (HOMO-1) and highest (HOMO) occupied MOs and the lowest (LUMO) and second-lowest (LUMO+1) unoccupied MOs, along with the differences in the respective orbitals ($E_{g-1} \equiv \Delta|\text{HOMO-1}| - |\text{HOMO}|$; $E_g \equiv \Delta|\text{HOMO}| - |\text{LUMO}|$; $E_{g+1} \equiv \Delta|\text{LUMO}| - |\text{LUMO+1}|$) for the calculated complexes of [*M*(cod)(*N*,*O*-Bid)]$^+$ [*M* = Ni^{II}, Pd^{II}, Pt^{II} (group 10 metals) and *N*,*O*-Bid = NH-acac, NMe-acac, NPh-acac] are presented in Figure 9.

In the HOMO-1 MOs of the NH-acac Ni-triad (Table S5, Supporting Information), the p orbitals seen on the carbon adjacent to the oxygen atoms of the NH-acac ligand, display an in-phase overlap of the metal orbitals with the alkene p orbitals of cod. For the HOMO MOs, π orbital delocalization on the NH-acac ligand is observed for all computed structures. On the other hand, for the LUMO MOs, $d_{x^2-y^2}$ orbitals are observed around the metal atoms, whereas for LUMO+1 MOs, a d_{z^2} orbital is clearly seen.

For the HOMO-1 MOs of the NMe-acac Ni-triad (Table S6, Supporting Information), an interesting feature is the p orbitals seen on the carbon adjacent to the oxygen atom of the NMe-acac ligand, with an in-phase overlap of the metal orbitals with the alkene p orbitals of the cyclooctadiene. This is continued to a lesser extent in the HOMO MOs with the orbitals shifting to the NMe-acac ligand, where the π delocalization on the back-bone is clearly visible. The central metal atoms have d_{yz} orbitals, whereas the p orbital of the methyl carbon of the NMe-acac ligand is seen. In the LUMO MOs, a $d_{x^2-y^2}$ orbital is observed centered on the metals of the group. The LUMO+1 MOs, tend to a d_{z^2} orbital centered on the metal.

In the HOMO-1 MOs of the NPh-acac Ni-triad (Table S7, Supporting Information), the π orbitals on the phenyl ring system are clearly observed. Similarly, for the HOMO MOs, π orbital delocalization on the NPh-acac ligand is observed for all computed structures, whereas for the LUMO MOs, $d_{x^2-y^2}$ orbitals are observed around the central metal atoms and for the LUMO+1 MOs, a d_{z^2} orbital is seen, i.e., it is continued

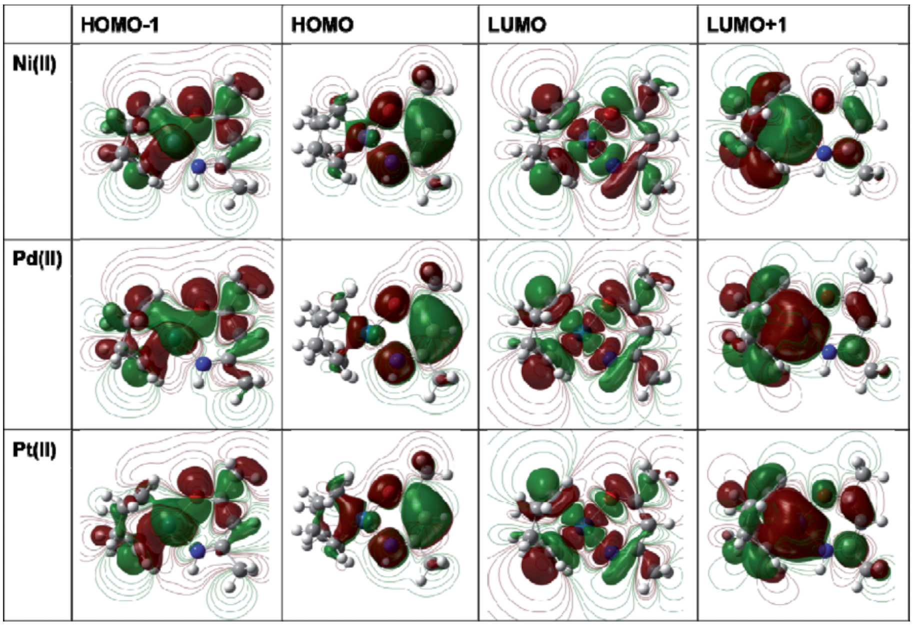

Figure 9. Molecular orbitals of calculated structures [*M*(cod)(NH-acac)]$^+$.

Table 4. Molecular orbital energies (Hartree) and energy gaps (eV) of the [*M*(cod)(*N*,*O*-Bid)]$^+$ (*M* = Ni^{II}, Pd^{II}, Pt^{II} and *N*,*O*-Bid = NH-acac, NMe-acac, NPh-acac) calculated structures.

	HOMO-1	HOMO	LUMO	LUMO+1	E_{g-1}	E_g	E_{g+1}
[*M*(cod)(NH-acac)]$^+$							
Ni^{II}	–0.40893	–0.35676	–0.23603	–0.18798	1.420	3.278	1.315
Pd^{II}	–0.40619	–0.35328	–0.22951	–0.18299	1.440	3.368	1.266
Pt^{II}	–0.40810	–0.35924	–0.19246	–0.18616	1.330	4.538	0.171
[*M*(cod)(NMe-acac)]$^+$							
Ni^{II}	–0.40565	–0.34794	–0.24074	–0.18502	1.570	2.917	1.516
Pd^{II}	–0.40513	–0.34509	–0.23256	–0.18095	1.634	3.062	1.404
Pt^{II}	–0.40713	–0.35095	–0.19542	–0.18401	1.529	4.232	0.310
[M(cod)(NPh-acac)]$^+$							
Ni^{II}	–0.36571	–0.34707	–0.23568	–0.17787	0.507	3.031	1.573
Pd^{II}	–0.36325	–0.34458	–0.22880	–0.17488	0.508	3.151	1.467
Pt^{II}	–0.36565	–0.35001	–0.19263	–0.17921	0.426	4.283	0.365

for all three ligand systems NH-acac, NMe-acac, and NPh-acac throughout the Ni-triad.

Table 4 presents the molecular orbital energies and energy gaps between the different corresponding MO levels in the [*M*(cod)(*N*,*O*-Bid)]$^+$ (*M* = Ni^{II}, Pd^{II}, Pt^{II} and *N*,*O*-Bid = NH-acac, NMe-acac, NPh-acac) calculated structures. The trends in particularly the energy gap (E_g) between the HOMO and LUMO MOs follow the typical increase from Ni^{II} to Pt^{II}, with Pd^{II} in between. Of interest is the fact that the NPh-acac complex lies between that of the NH-acac on the one side and the NMe-acac on the other.

Spectroscopy

In the spectra, which follow the peak assignments are denoted by the largest contributing vibration(s) to the band; the reported calculated frequencies are unscaled. The data is illustrated in Figure 10, with selected values reported in Table 5.

For the [*M*(cod)(*NH-acac*)]$^+$ complex, the band around 1610 cm^{-1} as seen in Figure 10a contains the ν(C=N), ν(C=C)$_{\text{NH-acac}}$, δ(CH), δ(NH), and γ(CH$_3$) vibrational contributions with the largest coming from ν(C=N). As can be seen there is not a significant difference in the frequencies when varying the metal atom for nickel, palladium, and platinum respectively. For the [*M*(cod)(NMe-acac)]$^+$ complex, the band around 1600 cm^{-1} (Figure 10b) contains the ν(C=N), ν(C=C)$_{\text{cod+NMe-acac}}$, δ(CH)$_{\text{cod+NMe-acac}}$, and γ(CH$_2$) vibrations with the largest fraction originating from ν(C=N). In Figure 10c the data for the [M(cod)(NPh-acac)]$^+$ complex is presented, where the band at 1590 cm^{-1} comprises ν(N=C), ν(C=C)$_{\text{NPh-acac+cod}}$, and δ(CH).

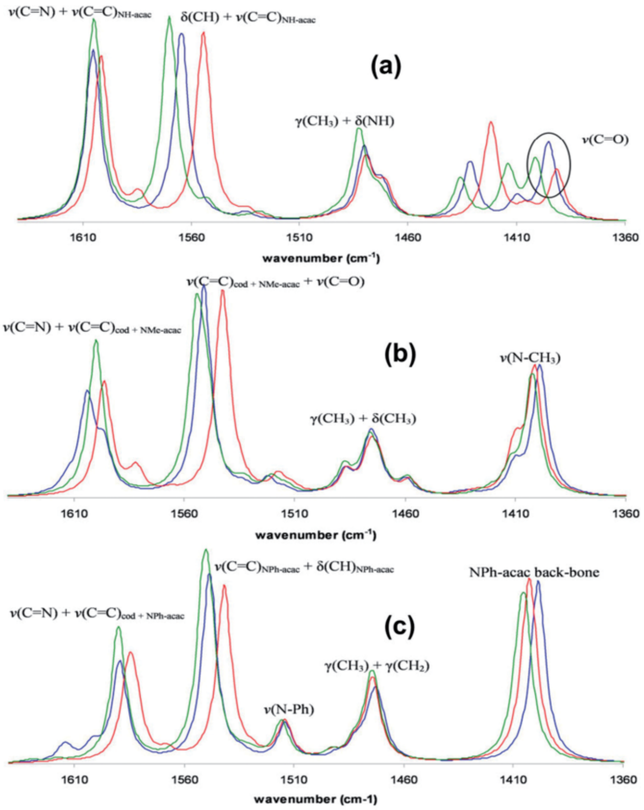

Figure 10. Calculated IR spectra of (a) [Ni(cod)(NH-acac)]$^+$ (blue), [Pd(cod)(NH-acac)]$^+$ (red), and [Pt(cod)(NH-acac)]$^+$(green); (b) [Ni(cod)(NMe-acac)]$^+$ (blue), [Pd(cod)(NMe-acac)]$^+$ (red), and [Pt(cod)(NMe-acac)]$^+$(green); (c) [Ni(cod)(NPh-acac)]$^+$ (blue), [Pd(cod)(NPh-acac)]$^+$ (red), and [Pt(cod)(NPh-acac)]$^+$(green). ν – stretching, δ – in-plane bending and γ – out-of-plane bending.

The ν(C=N) frequency for the complexes presented displays a difference of ca. 10 cm^{-1} indicating that the changing of the *R* group attached to the nitrogen atom does not significantly affect the vibration in the back-bone of the β-enaminonato ligands. A contributing factor to this is the conjugation therein

Table 5. Selected IR data /cm^{-1} for the Group 10 metal (Ni-Triad) complexes.

	[M(cod)(NH-acac)]$^+$			[M(cod)(NMe-acac)]$^+$			[M(cod)(NPh-acac)]$^+$		
	Ni	Pd	Pt	Ni	Pd	Pt	Ni	Pd	Pt
ν(C=N)	1605	1601	1605	1604	1595	1600	1589	1585	1590
ν(N–R) [a)]	1480	1480	1483	1399	1401	1402	1514	1514	1516

a) *R* = H, Me, Ph.

thus making the bonding character of the C–N, C–C, and C–O very similar, as reflected in the bond lengths (Table 1 and Table 2). It is interesting to note that a clearly defined band was observed for [*M*(cod)(NPh-acac)]$^+$ at 1401 cm^{-1} for this conjugated vibration. The ν(N–*R*) frequency is related to the inverse order of the electronegativity[13] (Ph, H, CH_3), thus as one decreases the electronegativity, the vibrational band shifts up-field.

Conclusions

The synthesis, characterization, and low temperature X-ray structures of six new β-enaminonato complexes of *cis*,*cis*-1,5-cyclooctadiene with Pd^{II} and Pt^{II} are reported, wherein the bonding arrangement of the cyclooctadiene ligand was critically evaluated based on different pre-defined parameters mimicking the geometric behavior of a Venus fly-trap as model.

A good correlation was found between the X-ray crystal structures and that of the DFT computed compounds. The bite (χ) and jaw (ψ) angles for both the solid-state crystal structures and the computed structures are presented, leading to the conclusion that upon varying the central metal atom in identical complexes down the nickel triad the jaw angle closes by ca. 8°. Further extended investigation into the Venus fly-trap angles for various β-enaminonato ligands as well as other transition metals will be required to formulate a more complete model of the bonding modes of cyclooctadiene.

The molecular orbital diagrams show the influence of both the p and d orbitals of the ligands as well as the central metal atoms. The comparison of the HOMO-1, HOMO, LUMO, and LUMO+1 MOs with those of the NH-acac, NMe-acac, and NPh-acac group 10 metal (Ni-triad) complexes shows a marked similarity. It is therefore concluded that the varying of the *R* group attached to the nitrogen of the β-enaminonato ligands does not play as significant a role as originally postulated.

The infra-red spectra showed that the change in the central metal atom exhibited not as a significant influence on the ν(C=N) stretching frequency as anticipated, however the electronegativity of the group attached to the nitrogen does have an influence on the ν(N–*R*) frequency.

Experimental Section

General: All reagents used for synthesis and characterization were of analytical grade, purchased from Sigma-Aldrich, unless otherwise stated. The metal complexes were purchased from Next Chimica (South Africa). Reagents were used as received, without purification.

Spectroscopy Measurements: NMR spectra were recorded with a Bruker Advance II 600 (^{1}H: 600.28 MHz; ^{13}C: 150.96 MHz), ^{1}H NMR spectra were referenced internally using residual protons in the deuterated solvent ($CDCl_3$: d 7.28; CD_2Cl_2: s 5.32). ^{13}C NMR spectra were similarly referenced internally to the solvent resonance ($CDCl_3$: t 77.36; CD_2Cl_2: m 53.8) with values reported relative to tetramethylsilane (d 0.0). Chemical shifts are reported in ppm. Infrared spectra were recorded with a Bruker Tensor 27 Standard System spectrophotometer with a laser range of 4000–370 cm^{-1}. Solid samples were prepared as potassium bromide disks.

Computational Methods: The DFT (density functional theory) molecular orbital calculations were carried out using the Gaussian 03[14] software suite. Becke's three parameter hybrid (B3LYP),[15,16] exchange correlation functional was used. The basis set employed in this study was 6-311++G(d,p)[17–19] for the main group elements and LanL2DZ[20] for the middle to late transition metals. Vibrational frequencies were calculated at the 6-311++G(d,p) level for the main group elements and at the LanL2DZ level for the middle to late transition metals with minimum energies confirmed to have zero imaginary frequencies. The frequencies were unscaled and used to compute the zero-point vibrational energies. The calculated harmonic wavenumbers were used in the analysis of the experimental IR spectra. DFT optimized structures of compounds not having crystal structures, are indicated by a "**C**" following the complexes' structure abbreviation and numbered **C1**–**C6**.

X-ray Crystal Structure Determinations: Data collections for [Pd(cod)(NH-acac)]BF_4 (**4**), [Pt(cod)(NH-acac)]PF_6 (**7**), [Pt(cod)(NMe-acac)]BF_4 (**8**), [Pt(cod)(NMe-acac)]PF_6 (**9**), and [Pt(cod)(NPh-acac)]PF_6 (**11**) were obtained with a Bruker APEX II 4 K CCD diffractometer. The data for [Pt(cod)(NH-acac)]BF_4 (**6**) and [Pt(cod)(NPh-acac)]BF_4 (**10**) were collected with an Oxford Diffraction Xcalibur 3 Crysalis CCD system.[21] All structures were collected at 100(2) K using Mo-K_α radiation (0.71073 Å). Both systems were equipped with a graphite-mono-chromatted Mo-K_α radiation, for the Bruker system all the reflections were merged and integrated with SAINT-PLUS[22] and corrected for Lorentz, polarization and absorption effects with SADABS,[23] whereas Crysalis RED[24] was used for the Oxford system.

Structures were solved by direct and conventional Patterson methods using SHELX-97[25] as part of the WinGX[26] package, and anisotropic refinement was performed on all non-hydrogen atoms by a full-matrix least-squares method on F^2. The positions of the hydrogen atoms were calculated using a riding model to the adjacent carbon, unless otherwise stipulated. Hydrogen interactions were calculated using the PLATON[27–29] and PARST[30] programs. Molecular graphics were obtained using DIAMOND,[31] while overlay illustrations were generated using HyperChem™ 7.5.[32] Details of the crystal data, intensity measurements and data processing are summarized in Table 6 for **4**, **6**–**10**, whereas selected bond lengths and angles are given in Table 2. Selected molecular structures with thermal ellipsoids (30 %) along with the general numbering scheme are presented in Figure 2; counterions are omitted for clarity and only selected hydrogen atoms are shown.

Crystallographic data (excluding structure factors) for the structures in this paper have been deposited with the Cambridge Crystallographic Data Centre, CCDC, 12 Union Road, Cambridge CB21EZ, UK. Copies of the data can be obtained free of charge on quoting the depository numbers CCDC-1473585 (**4**), CCDC-1473590 (**6**), CCDC-1473595 (**7**), CCDC-1473596 (**8**), CCDC-1473604 (**9**), and CCDC-1473630 (**10**) (Fax: +44-1223-336-033; E-Mail: deposit@ccdc.cam.ac.uk, http://www.ccdc.cam.ac.uk)

Synthesis of Dichlorido-1,5-cyclooctadieneplatinum(II): This was used as starting material and was prepared by the previously published method[8] by mixing of potassium tetrachloridoplatinate in water and propanol with *cis*,*cis*-1,5-cyclooctadiene (cod). Dichlorido-1,5-cyclooctadienepalladium(II)[9] was prepared by dissolving palladium dichloride in minimum of concentrated hydrochloric acid and diluting the solution with ethanol. To this was added cod with rapid stirring.

Table 6. Crystallographic data and refinement parameters for [*M*(cod)(LL′-Bid)]*A* (*M* = Pd, Pt, *A* = PF_6^- and BF_4^-, LL′-Bid = NH-acac, NMe-acac, NPh-acac).

	[Pd(cod)(NH-acac)]*A*	[Pt(cod)(NH-acac)]*A*		[Pt(cod)(NMe-acac)]*A*		[Pt(cod)(NPh-acac)]*A*
	BF_4 (**4**)	BF_4 (**6**)	PF_6 (**7**)	BF_4 (**8**) [a)]	PF_6 (**9**)	BF_4 (**10**)
Empirical formula	$C_{13}H_{20}BF_4NOPd$	$C_{13}H_{20}BF_4NOPt$	$C_{13}H_{20}F_6NOPPt$	$C_{14}H_{22}BF_4NOPt$	$C_{14}H_{22}F_6NOPPt$	$C_{19}H_{24}BF_4NOPt$
FW	399.51	488.20	546.36	502.23	560.39	564.29
Crystal system	monoclinic	monoclinic	monoclinic	orthorhombic	monoclinic	monoclinic
Space group	$P2_1/c$	$P2_1/c$	$C2/m$	$P2_12_12_1$	$C2/m$	$P2_1/c$
a /Å	9.8665(3)	9.8588(2)	26.8871(12)	7.5277(2)	26.5792(6)	9.5952(7)
b /Å	12.7836(3)	12.8652(2)	7.1009(3)	13.9653(4)	7.19030(10)	21.2609(16)
c /Å	12.7126(3)	12.6969(3)	8.7130(4)	14.7872(4)	9.3146(2)	10.3336(6)
α /°	90	90	90	90	90	90
β /°	110.851(1)	111.040(2)	105.305(3)	90	106.250(1)	117.664(5)
γ /°	90	90	90	90	90	90
V /Å^3	1498.42(7)	1503.05(5)	1604.51(12)	1554.53(7)	1709.02(6)	1867.1(2)
Z	4	4	4	4	4	4
D_{calc} /Mg·m^{-3}	1.771	2.157	2.262	2.146	2.178	2.007
μ /mm^{-1}	1.278	9.375	8.908	9.068	8.366	7.562
F(000)	800	928	1040	960	1072	1088
Crystal size /mm^3	0.42 × 0.19 × 0.05	0.26 × 0.15 × 0.13	0.19 × 0.17 × 0.10	0.35 × 0.15 × 0.08	0.38 × 0.13 × 0.04	0.26 × 0.23 × 0.10
θ range /°	3.35 to 28.00	2.34 to 30.00	1.57 to 28.48	3.04 to 28.37	3.19 to 28.30	2.42 to 28.00
Index ranges	$-13 \le h \le 12$, $-16 \le k \le 16$, $-16 \le l \le 16$	$-13 \le h \le 9$, $-17 \le k \le 18$, $-16 \le l \le 17$	$-35 \le h \le 35$, $-9 \le k \le 9$, $-11 \le l \le 11$	$-6 \le h \le 9$, $-18 \le k \le 18$, $-19 \le l \le 19$	$-35 \le h \le 35$, $-6 \le k \le 9$, $-12 \le l \le 12$	$-12 \le h \le 12$, $-27 \le k \le 28$, $-8 \le l \le 13$
Reflections collected	17329	13378	18461	28496	14798	14547
Independent reflections	3611 [R_{int} = 0.0266]	4374 [R_{int} = 0.0226]	2167 [R_{int} = 0.1076]	3853 [R_{int} = 0.0403]	2296 [R_{int} = 0.0413]	4398 [R_{int} = 0.0644]
Complete θ /°,%	28.00, 99.9	30.00, 100.0	28.48, 98.9	28.37, 99.4	28.30, 99.7	28.00, 97.7
Max/min. trans	0.9389 / 0.6159	0.3754 / 0.1942	0.4695 / 0.2824	0.5307 / 0.1435	0.7308 / 0.1432	0.5185 / 0.2438
Data/ restraints/ parameters	3611 / 0 / 215	4374 / 0 / 196	2167 / 0 / 124	3853 / 0 / 202	2296 / 191 / 159	4398 / 0 / 246
GoF on F^2	1.068	1.003	1.252	1.044	1.042	0.991
Final R indices [$I > 2\sigma(I)$]	R_1 = 0.0210, wR_2 = 0.0509	R_1 = 0.0209, wR_2 = 0.0490	R_1 = 0.0381 wR_2 = 0.0787	R_1 = 0.0148	R_1 = 0.0205	R_1 = 0.0332, wR_2 = 0.0805
R indices (all data)	R_1 = 0.0241, wR_2 = 0.0525	R_1 = 0.0283, wR_2 = 0.0507	R_1 = 0.0410, wR_2 = 0.0802	R_1 = 0.0154	R_1 = 0.0226	R_1 = 0.0389, wR_2 = 0.0823
Largest diff. peak/ hole /e·Å^{-3}	0.507 and –0.450	2.427 and –0.952	1.440 and –1.925	0.912 and –0.713	0.621 and –0.966	3.323 and –2.601

a) Flack parameter = 0.006(5).

Synthesis of Ligands: 4-Aminopent-3-en-2-one [HNH-acac] (1): A solution of acetylacetone (11 g, 0.11 mol), NH_4OH (28 % in H_2O, 12.5 g, 0.1 mol) and 2 drops H_2SO_4 (conc.) in benzene (100 mL) was refluxed overnight in a Dean Stark setup. The solution was filtered, and the solvent removed on a rotary evaporator where upon the oil of **1** was allowed to stand overnight. Yield 9.7 g (89 %). **IR** (KBr): ṽ = νC=O 1700, νN–H 3338 cm^{-1}. **^{1}H NMR** (600.28 MHz, $CDCl_3$): δ = 1.911 (s, 3 H, CH_3), 2.033 (s, 3 H, CH_3), 5.032 (s, 1 H, CH), 9.701 (s, 1 H, NH). **^{13}C{^{1}H} NMR** (150.96 MHz, $CDCl_3$): δ = 22.56 (CH_3), 29.53 (CH_3), 96.08 (CH), 161.27 (CNH), 197.07 (CO).

4-(Methylamino)pent-3-en-2-one [HNMe-acac] (2): An analogous method as described for **1** was used in the preparation of **2** replacing NH_4OH with H_2NCH_3 (40 % in H_2O, 7.76 g, 0.1 mol). Yield 8.9 g (72 %). **^{1}H NMR** (600.28 MHz, $CDCl_3$): δ = 1.918 (s, 3 H, CH_3), 1.970 (s, 3 H, CH_3), 2.932 (d, 3 H, CH_3, J = 4.8 Hz), 4.981 (s, 1 H, CH), 10.699 (s, 1 H, NH) **^{13}C{^{1}H} NMR** (150.96 MHz, $CDCl_3$): δ = 18.97 (CH_3), 28.95 (CH_3), 29.77 (CH_3), 95.43 (CH), 164.55 (CNH), 195.01 (CO).

4-Anilinopent-3-en-2-one [HNPh-acac] (3): An analogous method as described for **1** was used in the preparation of **3** replacing NH_4OH with aniline (9.31 g, 0.1 mol). Yield 15.4 g (80 %). **IR** (KBr): ṽ = νC=O 1606, νN–H 3050 cm^{-1}. **^{1}H NMR** (600.28 MHz, $CDCl_3$): δ = 2.005 (s, 3 H, CH_3), 2.113 (s, 3 H, CH_3), 5.201 (s, 1 H, CH), 7.12 (d, 2 H, CH, J = 7.2 Hz), 7.203 (t, 1 H, CH, J = 7.2 Hz), 7.35 (t, 2 H, CH, J = 7.2 Hz), 12.486 (s, 1 H, NH). **^{13}C{^{1}H} NMR** (150.96 MHz, $CDCl_3$): δ = 20.15 (CH_3), 29.49 (CH_3), 97.91 (CH_3), 125.07 (CH), 125.87 (CH), 129.4 (CH), 139.06 (CH), 160.56 (CNH), 196.45 (CO).

Synthesis of the Complexes: [Pd(cod)(NH-acac)]BF_4 (4): Using a modified synthetic procedure,[33] [Pd(cod)Cl_2] (100 mg, 0.35 mmol) was dissolved in DCM (5 mL). To this $AgBF_4$ (136 mg, 0.7 mmol) was added and the resulting solution was stirred for ca. 15 min. An equivalent of **1** (31 µL, 0.35 mmol) was added and the mixture stirred for a few min to allow the reaction to complete. The solution was filtered and Et_2O was added (ca. 20 mL) to the filtrate to precipitate **4**. The resulting solution was again filtered and the precipitate washed with Et_2O (3 × 3 mL) portions. Crystals suitable for X-ray diffraction were obtained by DCM / Et_2O vapor diffusion. Yield 36 mg (24 %). **IR** (KBr): ṽ = νN–H 3314, νC=C 1589, νC=O 1708, νPd–O 717 and 476, νPd–[C=C] 522 cm^{-1}. **^{1}H NMR** (600.28 MHz, CD_2Cl_2): δ = 2.086 (s, 3 H, CH_3), 2.231 (s, 3 H, CH_3), 2.681 (m, 4 H, CH_2), 2.884 (m, 4 H, CH_2), 5.216 (d, 1 H, CH, J = 2.4 Hz), 6.111 (m, 2 H, CH), 6.222 (m, 2 H, CH). **^{13}C{^{1}H} NMR** (150.96 MHz, CD_2Cl_2): δ = 24.91 (CH_3), 24.84 (CH_3), 28.93 (CH_2), 31.08 (CH_2), 97.25 (CH), 110.76 (CH), 118.82 (CH), 166.24 (CN), 177.4 (CO).

[Pd(cod)(NH-acac)]PF_6 (5): The compound was prepared in a similar manner as described for **4**, except $AgPF_6$ (177 mg, 0.7 mmol) was used instead of $AgBF_4$. Yield 32 mg (21 %). **IR** (KBr): $\tilde{\nu}$ = νN–H 3368, νC=C 1582, νC=O 1699, νPd–O 692 and 474, νPd–[C=C] 557 cm^{-1}. **^{1}H NMR** (600.28 MHz, CD_2Cl_2): δ = 2.097 (s, 3 H, CH_3), 2.220 (s, 3 H, CH_3), 2.698 (m, 4 H, CH_2), 2.891 (m, 4 H, CH_2), 5.239 (d, 1 H, CH, J = 2.4 Hz), 6.127 (m, 4 H, CH). **^{13}C{^{1}H} NMR** (150.96 MHz, CD_2Cl_2): δ = 24.93 (CH_3), 25.15 (CH_3), 28.97 (CH_2), 31.05 (CH_2), 97.31 (CH), 110.76 (CH), 119.08 (CH), 166.36 (CN), 178.01 (CO).

[Pt(cod)(NH-acac)]BF_4 (6): An analogous method as described for **4** was used in the preparation of **6** replacing [Pd(cod)Cl_2] with [Pt(cod)Cl_2] (100 mg, 27 mmol). Crystals suitable for X-ray diffraction were obtained by DCM / Et_2O vapor diffusion. Yield 55 mg (41 %). **IR** (KBr): $\tilde{\nu}$ = νC=C 1539, νC=O 1587, νPt–O 664 and 470, νPt–[C=C] 521 cm^{-1}. **^{1}H NMR** (600.28 MHz, CD_2Cl_2): δ = 2.136 (s, 3 H, CH_3), 2.281 (s, 3 H, CH_3), 2.508 (m, 4 H, CH_2), 2.718 (m, 4 H, CH_2), 5.428 (d, 1 H, CH, J = 2.4 Hz), 5.658 (dt, 4 H, CH, J = 3 Hz, 15.6 Hz), 9.212 (s, 1 H, NH). **^{13}C{^{1}H} NMR** (150.96 MHz, CD_2Cl_2): δ = 25.55 (d, CH_3, J = 7.5 Hz), 28.76 (CH_3), 30.06 (CH_2), 31.09 (CH_2), 92.28 (CH), 100.01 (CH), 102.51 (CH), 166.48 (CN), 177.57 (CO).

[Pt(cod)(NH-acac)]PF_6 (7): The compound was prepared in a similar manner as described for **6**, replacing the $AgBF_4$ with $AgPF_6$ (135 mg, 27 mmol). Crystals suitable for X-ray diffraction were obtained by DCM / Et_2O vapor diffusion. Yield 91 mg (60 %). **IR** (KBr): $\tilde{\nu}$ = νC=C 1539, νC=O 1587, νPt–O 664 and 471, νPt–[C=C] 557 cm^{-1}. **^{1}H NMR** (600.28 MHz, CD_2Cl_2): δ = 2.147 (2, 3 H, CH_3), 2.269 (s, 3 H, CH_3), 2.522 (m, 4 H, CH_2), 2.725 (m, 4 H, CH_2), 5.325 (d, 1 H, CH, J = 6.6 Hz), 5.627 (dt, 4 H, CH, J = 33 Hz, 57 Hz), 8.601 (s, 1 H, NH). **^{13}C{^{1}H} NMR** (150.96 MHz, CD_2Cl_2): δ = 25.66 (d, CH_3, J = 28.7 Hz), 28.76 (CH_3), 29.95 (CH_2), 31.04 (CH_2), 92.21 (CH), 99.78 (d, CH, J = 83 Hz), 102.79 (CH), 166.51 (NH), 178.15 (CO).

[Pt(cod)(NMe-acac)]BF_4 (8): Using the preparation method as described for compound **6**, ligand **1** was replaced with ligand **2** (31.9 µL, 27 mmol). Crystals suitable for X-ray diffraction were obtained by DCM / Et_2O vapor diffusion. Yield 96 mg (70 %). **IR** (KBr): $\tilde{\nu}$ = νC=C 1522, νC=O 1584, νPt–O 635 and 416, νPt–[C=C] 521, νPt–N 472 cm^{-1}. **^{1}H NMR** (600.28 MHz, CD_2Cl_2): δ = 2.117 (s, 3 H, CH_3), 2.228 (s, 3 H, CH_3), 2.485 (m, 2 H, CH_2), 2.607 (m, 2 H, CH_2), 2.734 (m, 2 H, CH_2), 2.890 (m, 2 H, CH_2), 3.315 (t, 3 H, CH_3, J = 12.6 Hz), 5.450 (s, 1 H, CH), 5.486 (sep 2 H, CH, J = 19.8 Hz, 7.8 Hz, 3 Hz), 5.791 (sep, 2 H, CH, J = 14.4 Hz, 9 Hz, 3 Hz). **^{13}C{^{1}H} NMR** (150.96 MHz, CD_2Cl_2): δ = 24.62 (CH_3), 24.97 (CH_3), 28.22 (CH_2), 31.84 (CH_2), 42.69 (CH), 97.32 (CH), 102.17 (CH), 104.83 (CH), 167.45 (CN), 174.94 (CO).

[Pt(cod)(NMe-acac)]PF_6 (9): The compound was prepared in a similar manner as described for **8**, replacing the $AgBF_4$ with $AgPF_6$ (135 mg, 27 mmol). Crystals suitable for X-ray diffraction were obtained by DCM / Et_2O vapor diffusion. Yield 125 mg (82 %). **IR** (KBr): $\tilde{\nu}$ = νC=C 1518, νC=O 1580, νPt–O 636 and 419, νPt–[C=C] 557, νPt–N 467 cm^{-1}. **^{1}H NMR** (600.28 MHz, CD_2Cl_2): δ = 2.120 (s, 3 H, CH_3), 2.224 (s, 3 H, CH_3), 2.483 (m, 2 H, CH_2), 2.602 (m, 2 H, CH_2), 2.731 (m, 2 H, CH_2), 2.881 (m, 2 H, CH_2), 3.299 (t, 3 H, CH_3, J = 12.6 Hz), 5.454 (s, 1 H, CH), 5.448 (sep, 2 H, CH, J = 22.2 Hz, 8.4 Hz, 3 Hz), 5.797 (sep, 2 H, CH, J = 14.4 Hz, 8.4 Hz, 3 Hz). **^{13}C{^{1}H} NMR** (150.96 MHz, CD_2Cl_2): δ = 24.61 (CH_3), 24.94 (CH_3), 28.2 (CH_2), 31.21 (CH_2), 42.59 (CH_3), 97.16 (CH), 102.17 (CH), 104.89 (CH), 167.46 (CN), 175.01 (CO).

[Pt(cod)(NPh-acac)]BF_4 (10): Using the preparation method as described for compound **6**, ligand **2** was replaced with ligand **3** (47 mg, 27 mmol). Crystals suitable for X-ray diffraction were obtained by DCM / Et_2O vapor diffusion. Yield 85 mg (55 %). **IR** (KBr): $\tilde{\nu}$ = νC=C 1518, νC=O 1566, νPt–O 659 and 474, νPt–[C=C] 522, νPt–N 548 cm^{-1}. **^{1}H NMR** (600.28 MHz, CD_2Cl_2): δ = 1.806 (s, 3 H, CH_3), 2.228 (s, 3 H, CH_3), 2.392 (m, 4 H, CH_2), 2.696 (m, 4 H, CH_2), 4.712 (sep, 2 H, CH, J = 18.6 Hz, 8.4 Hz, 3 Hz), 5.619 (s, CH), 5.869 (sep, 2 H, CH, J = 15 Hz, 9 Hz, 2.4 Hz), 7.037 (d, 2 H, CH, J = 7.2 Hz), 7.34 (t, 1 H, CH, J = 7.8 Hz), 7.514 (t, 2 H, CH, J = 7.8 Hz). **^{13}C{^{1}H} NMR** (150.96 MHz, CD_2Cl_2): δ = 24.9 (CH_3), 25.43 (CH_3), 28.03 (CH_2), 30.77 (d, CH_2, J = 25.6 Hz), 98.33 (CH), 101.45 (CH), 104.43 (CH), 146.91 (CN), 166.23 (CN), 177.35 (CO).

[Pt(cod)(NPh-acac)]PF_6 (11)[34]: The compound was prepared in a similar manner as described for **10**, replacing the $AgBF_4$ with $AgPF_6$ (135 mg, 27 mmol). Crystals suitable for X-ray diffraction were obtained by DCM / Et_2O vapor diffusion. Yield 132 mg (78 %). **IR** (KBr): $\tilde{\nu}$ = νC=C 1519, νC=O 1563, νPt–O 658 and 473, νPt–[C=C] 557, νPt–N 525 cm^{-1}. **^{1}H NMR** (600.28 MHz, CD_2Cl_2): δ = 1.804 (s, 2 H, CH_3), 2.227 (s, 3 H, CH_3), 2.387 (m, 4 H, CH_2), 2.722 (m, 4 H, CH_2), 4.705 (sep, 2 H, CH, J = 20.4 Hz, 9 Hz, 2.4 Hz), 5.619 (s, 1 H, CH), 5.866 (sep, 2 H, CH, J = 14.4 Hz, 9 Hz, 2.4 Hz), 7.03 (s, 2 H, CH, J = 7.8 Hz), 7.34 (t, 1 H, CH, J = 7.2 Hz), 7.513 (t, 2 H, CH, J = 7.8 Hz). **^{13}C{^{1}H} NMR** (150.96 MHz, CD_2Cl_2): δ = 25.27 (CH_3), 25.8 (CH_3), 28.4 (CH2), 31.05 (CH2), 98.68 (CH), 101.83 (CH), 104.81 (CH), 125.51 (CH), 128.73 (CH), 130.25 (CH), 147.29 (CN), 166.62 (CN), 177.76 (CO).

Supporting Information (see footnote on the first page of this article): Figures and Tables (21pp) are provided giving additional X-Ray results, Computed Orbitals as well as NMR and IR spectra.

Acknowledgements

Financial assistance from the University of the Free State is gratefully acknowledged. We thank *Prof. Ola Wendt* from the University of Lund, Sweden for the use of their Oxford X-ray diffractometer. We also express our gratitude to SASOL, the South African National Research Foundation (SA-NRF/THRIP), the Inkaba yeAfrica initiative, the UFS Strategic Cluster Initiative (Materials and Nonosciences), the Swedish International Development Co-operation Agency (SIDA), and the Swiss NSF for financial support of this project. Part of this material is based on work supported by the SA-NRF/ THRIP under grant number GUN2068915 and GUN107802. Opinions, findings, conclusions or recommendations expressed in this material are those of the authors and do not necessarily reflect the views of the SA-NRF.

Keywords: Palladium; Platinum; Cyclooctadiene; X-ray crystallography; Density functional calculations; Venus fly-trap

References

[1] C. A. Buehler, D. E. Pearson, *Survey of Organic Synthesis*, vol 1, Wiley-Interscience, New York, **1970**.

[2] G. Oenbrink, T. Schiffer, *Cyclododecatriene, Cyclooctadiene, and 4-Vinylcyclohexene*, in *Ullmann's Encyclopedia of Industrial Chemistry*, Evonik Degussa GmbH, Marl, Germany, **2009**.

[3] a) A. Roodt, S. Otto, G. Steyl, *Coord. Chem. Rev.* **2003**, *245*, 125–142; b) A. Brink, H. G. Visser, A. Roodt, G. Steyl, *Dalton Trans.* **2010**, *39*, 5572–5578; c) M. T. Johnson, R. Johansson, M. V. Kondrashov, G. Steyl, M. S. G. Ahlquist, A. Roodt, O. F. Wendt, *Organometallics* **2010**, *29*, 3521–3529.

[4] a) C. Sacht, M. S. Datt, S. Otto, A. Roodt, *J. Chem. Soc., Dalton Trans.* **2000**, 4579–4586; b) M. J. Johansson, S. Otto, A. Roodt, Å. Oskarsson, *Acta Crystallogr., Sect. B* **2000**, *56*, 226–233; c) C. Sacht, M. S. Datt, S. Otto, A. Roodt, *J. Chem. Soc., Dalton Trans.* **2000**, *5*, 727–733; d) S. Otto, A. Roodt, *Inorg. Chem. Comm.* **2001**, *4*, 47; e) S. Otto, A. Roodt, L. I. Elding, *Inorg. Chem. Commun.* **2006**, *9*, 764–766; f) S. Otto, A. Roodt, K. I. Elding, *Inorg. Chem. Commun.* **2009**, *12*, 766–768; g) A. Roodt, H. G. Visser, A. Brink, *Crystallogr. Rev.* **2011**, *17*, 241–280.
[5] R. H. Crabtree, *The Organometallic Chemistry of Transition Metals*, 4th ed., John Wiley & Sons Inc., Hoboken, New Jersey, **2005**.
[6] D. Schnell, P. Catling, G. Folkerts, C. Frost, R. Gardner et al., *Dionaea muscipula* The IUCN Red List of Threatened Species, **2000**: e.T3936A10253384, Taxonomic Serial No. (ITIS): 22008, http://dx.doi.org/10.2305/IUCN.UK.2000.RLTS.T39636A10253384.en (accessed March 2018).
[7] a) T. N. Hill, G. Steyl, A. Roodt, *Polyhedron* **2013**, *50*, 82–89; b) T. N. Hill, G. Steyl, A. Roodt, *Acta Crystallogr., Sect. B* **2013**, *69*, 36–42.
[8] S. Otto, *Structural and Reactivity Relationships in Platinum(II) and Rhodium(I) complexes*, PhD Thesis, University of the Free State, Bloemfontein, South Africa, **1999**.
[9] A. M. M. Meij, PhD Thesis, Rand Afrikaans University, Johannesburg, South Africa, **2004**.
[10] T. N. Hill, A. Roodt, G. Steyl, *Acta Crystallogr., Sect. B* **2013**, *69*.
[11] CSD, ver 5.36: C. R. Groom, I. J. Bruno, M. P. Lightfoot, S. C. Ward, *Acta Crystallogr., Sect. B* **2016**, *72*, 171–179.
[12] J. L. Boyer, T. R. Cundari, N. J De Yonker, T. B. Rauchfuss, S. R. Wilson, *Inorg. Chem.* **2009**, *48*, 638–645.
[13] P.-C. Nam, M. T. Nguyen, A. K. Chandra, *J. Phys. Chem. A* **2006**, *110*, 4509–4515.
[14] M. J. Frisch, G. W. Trucks, H. B. Schlegel, G. E. Scuseria, M. A. Robb, J. R. Cheeseman, J. A. Montgomery Jr., T. Vreven, K. N. Kudin, J. C. Burant, J. M. Millam, S. S. Iyengar, J. Tomasi, V. Barone, B. Mennucci, M. Cossi, G. Scalmani, N. Rega, G. A. Petersson, H. Nakatsuji, M. Hada, M. Ehara, K. Toyota, R. Fukuda, J. Hasegawa, M. Ishida, T. Nakajima, Y. Honda, O. Kitao, H. Nakai, M. Klene, X. Li, J. E. Knox, H. P. Hratchian, J. B. Cross, V. Bakken, C. Adamo, J. Jaramillo, R. Gomperts, R. E. Stratmann, O. Yazyev, A. J. Austin, R. Cammi, C. Pomelli, J. W. Ochterski, P. Y. Ayala, K. Morokuma, G. A. Voth, P. Salvador, J. J. Dannenberg, V. G. Zakrzewski, S. Dapprich, A. D. Daniels, M. C. Strain, O. Farkas, D. K. Malick, A. D. Rabuck, K. Raghavachari, J. B. Foresman, J. V. Ortiz, Q. Cui, A. G. Baboul, S. Clifford, J. Cioslowski, B. B. Stefanov, G. Liu, A. Liashenko, P. Piskorz, I. Komaromi, R. L. Martin, D. J. Fox, T. Keith, M. A. Al-Laham, C. Y. Peng, A. Nanayakkara, M. Challacombe, P. M. W. Gill, B. Johnson, W. Chen, M. W. Wong, C. Gonzalez, J. A. Pople, Gaussian 03, Revision E.01, Gaussian Inc., Wallingford CT, **2004**.
[15] A. D. Becke, *J. Chem. Phys.* **1993**, *98*, 5648–5652.
[16] C. Lee, W. Yang, R. G. Parr, *Phys. Rev. B* **1988**, *37*, 785–789.
[17] R. Ditchfield, W. J. Hehre, J. A. Pople, *J. Chem. Phys.* **1971**, *54*, 724–728.
[18] M. S. Gordon, *Chem. Phys. Lett.* **1980**, *76*, 163–168.
[19] V. A. Rassolov, M. A. Ratner, J. A. Pople, P. C. Redfern, L. A. Curiss, *J. Comput. Chem.* **2001**, *22*, 976–984.
[20] P. J. Hay, W. R. Wadt, *J. Chem. Phys.* **1985**, *82*, 299–310.
[21] Crysalis CCD, Oxford Diffraction Ltd., Abingdon, Oxfordshire, U. K., **2005**.
[22] Bruker *SAINT-PLUS* (including XPREP), Version 7.12, Bruker AXS Inc., Madison, WI., **2004**.
[23] Bruker *SADABS* (Version 2004/1), Bruker ASX Inc., Madison, WI., **1998**.
[24] Crysalis RED Oxford Diffraction Ltd., Abingdon, Oxfordshire, U. K., **2005**.
[25] G. M. Sheldrick, *Acta Crystallogr., Sect. A* **2008**, *64*, 112–122.
[26] L. J. Farrugia, *Appl. Crystallogr.* **1999**, *32*, 837–838.
[27] A. L. Spek, *PLATON A Multipurpose Crystallographic Tool*, Utrecht University, Utrecht, Netherlands, **2005**.
[28] A. L. Spek, *J. Appl. Crystallogr.* **2003**, *36*, 7–13.
[29] A. L. Spek, *Acta Crystallogr., Sect. D* **2009**, *65*, 148–155.
[30] M. Nardelli, *J. Appl. Crystallogr.* **1995**, *28*, 659–660.
[31] K. Brandenburg, M. Brendt, DIAMOND, Release 2.1e, Crystal Impact GbR, Potfach 1251, D53002 Bonn, Germany, **2001**.
[32] HyperChem™ Release 7.52, Windows Molecular Modeling System, HyperCube Inc., **2002**.
[33] D. A. White, *Inorg. Synth.* **1972**, *13*, 55–65.
[34] T. N. Hill, A. Roodt, CCDC 1473640, *CSD Communication*, **2016**.

Received: March 15, 2018